International Journal of Control, Automation, and Systems (2013) 11(4):718-727 ISSN:1598-6446 eISSN:2005-4092
DOI 10.1007/s12555-012-9305-z http://www.springer.com/12555

Partial Feedback Linearization Control of a Three-Dimensional Overhead Crane

Le Anh Tuan, Soon-Geul Lee*, Viet-Hung Dang, Sangchan Moon, and ByungSoo Kim

Abstract: Based on partial feedback linearization, an improved nonlinear controller is analyzed and designed for the three-dimensional motion of an overhead crane. Three control inputs composed of bridge moving, trolley travelling, and cargo hoisting forces are used to drive five state variables consisting of bridge motion, trolley movement, cargo hoisting displacement, and two cargo swing angles. The control scheme is constituted by linearly combining two components that are separately obtained from the nonlinear feedback of actuated and un-actuated states. To verify the quality of the control process, both numerical simulation and experimental study are carried out. The proposed controller asymptotically stabilizes all system states.

Keywords: Internal dynamics, overhead cranes, partial feedback linearization, system stability.

1. INTRODUCTION

Cargo transportation plays an important role in many industrial fields today. For the transport of cargo over short distances or to small areas, such as automotive factories and shipyards, overhead cranes are naturally applied. In high-speed operations, overhead cranes are required to increase productivity. However, the fast motion of overhead cranes usually causes large swinging movements of cargo and non-precise movements of the trolley and bridge. This characteristic makes the operating process dangerous and unsafe. Therefore, a modern overhead crane system is normally equipped with a good control strategy to reduce the swinging of cargo and to increase the precision of crane motions. Thus far, the control problems of overhead and container cranes [1-3] in both theory and practice have attracted the attention of many researchers, prompting their use of various control techniques that range from the classical methods [4-8] to the modern techniques [9-12].

Several approaches, such as sliding mode control (SMC) [13-17], feedback linearization control (FLC), Lyapunov design [18-20], optimal nonlinear control [21], adaptive control [22-25], energy-based design [26], and geometric analysis [27], have been proposed for the nonlinear control of crane systems. The present study pursues the control of crane systems using FLC. Park *et al*. [28] provided a nonlinear controller for a 2D container crane to suppress the cargo swing, track the trolley, and to lift the cargo. The FLC technique was partially applied to actuated dynamics (characterized for trolley moving and cargo hoisting forces) to obtain one component of the controller. Meanwhile, the anti-swing component was obtained from an energy-based nonlinear control design. Borges *et al*. [29] used a state observer-controller for the anti-swing component of a payload using input-output feedback linearization. Bobasu *et al*. [30] designed an exact linearization feedback control law for a nonlinear crane by combining input-output linearization and a few nonlinear adaptive control techniques. Two papers of Chen *et al*. on 2D overhead cranes [31] and 3D crane systems [32] dealt with nonlinear control using an input-state linearization technique. In [31], the control law was obtained from the nonlinear feedback of actuated states (trolley moving and cargo lifting forces) without considering the un-actuated state (cargo swing angle). Therefore, this control scheme could not suppress the cargo vibration. The control scheme in [32], as an improvement of that in [31], was designed based on the partial feedback linearization (PFL) of actuated states. Furthermore, the damped component for reducing the cargo swings was added to the control law. Cho and Lee [33] recently proposed a control scheme linearly composed of a nominal and corrective PD control, with the nominal PD control law designed through feedback linearization. Cho el al. [34] also extended the PFL-based controller in [33], wherein the adaptive component was integrated.

Manuscript received July 8, 2012; revised December 12, 2012 and February 3, 2013; accepted March 25, 2013. Recommended by Editorial Board member Pinhas Ben-Tzvi under the direction of Editor Hyouk Ryeol Choi.

This research was supported by the IT R&D program of MKE/KEIT [KI10040990, A Development of Communication Technology with UTIS & Vehicle Safety Support Service for Urban Area] and by the Implementation of Technologies for Identification, Behavior, and Location of Human based on Sensor Network Fusion Program through the MKE (Grant Number: 10041629). It also was supported by the Technology Innovation Program (10040992) of MKE/KEIT.

Le Anh Tuan and Viet-Hung Dang are with the Research and Development Center of Duy Tan University, Da Nang city, Vietnam (e-mails: {vimaru1980, dangviethungha}@gmail.com).

Soon-Geul Lee, Sangchan Moon, and ByungSoo Kim are with Kyung Hee Univ., 1 Seocheon-dong, Giheung-gu, Yongin-si, Gyeonggi-do 449-701, Korea (e-mails: sglee@khu.ac.kr, lovemeje @hanmail.net, poposoo@chol.com).

* Corresponding author.

Based on [28,31,32], we design an upgraded nonlinear controller in which the PFL technique is applied for both actuated dynamics (characterized for trolley and bridge as well as cargo lifting motions) and un-actuated one (characterized for cargo swings). Unlike the controllers of Park *et al*. [28] and Chen *et al*. [31,32], the proposed control scheme is linearly composed of two components that are separately obtained from the states' nonlinear feedback of actuated dynamics and from the PFL of un-actuated dynamics. First, a system dynamics of overhead cranes composed of five highly nonlinear second order differential equations is created. The system involves two un-actuated states and three actuated states driven by three control inputs. A 3D overhead crane is an under-actuated system. Therefore, its system dynamics should be separated into actuated and un-actuated models. Next, the actuated dynamics is "linearized" using a nonlinear feedback technique; thus, the un-actuated model is considered as internal dynamics. Considering actuated states as system outputs, a nonlinear controller is then proposed to track the output trajectories to the desired values. However, this nonlinear control scheme does not guarantee the convergence of un-actuated states. Therefore, its structure should be modified to satisfy the stability condition of both the actuated and un-actuated states based on the feedback linearization of all system states. The controller structure is now the linear combination of two components that are separately obtained from the feedback linearization of the actuated dynamics and of the un-actuated model.

Compared with traditional controllers such as the PID controller, the PFL controller has several advantages. In the design of the PID controller, almost all nonlinear factors of a system are not considered. Meanwhile, in the design of the PFL controller, all nonlinearities of a system mentioned on the mathematical model are completely suppressed by the PFL control law. However, the PFL approach requires a precise model to achieve good control action. Furthermore, it is not useful in systems with uncertain parameters. The study aims to design a controller that asymptotically pulls all system responses to the desired values.

It is structured as follows. In Section 2, a highly nonlinear mathematical model is generated based on the Lagrange equation for overhead cranes that involve complicated operations. Section 3 describes the design of the nonlinear controller, which involves the decoupling of the system dynamics, design of the control law based on PFL, and the analysis of system stability. The simulation of system responses, real-time experiment, and the result analysis are given in Section 4. Finally, conclusions and remarks are discussed in Section 5.

2. SYSTEM DYNAMICS

The crane system comprising four masses is physically modeled in Fig. 1. The distributed masses of the bridge are converted into a concentrated mass m_b placed in the bridge center. m_l denotes the equivalent masses of the hoist mechanism, while m_t and m_c are masses of the trolley and cargo, respectively. The overhead crane has five degrees of freedom corresponding to five generalized coordinates: $x(t)$ is the trolley displacement, $z(t)$ indicates the bridge motion along the Oz axis, and the cargo position is determined by three generalized coordinates (l, θ, φ), where θ and φ are projections of the swing angle on the ABC and ABD planes, respectively. Hence, the generalized coordinates of the system are characterized by vector $\mathbf{q}=[z \quad x \quad l \quad \varphi \quad \theta]^T$. In addition, the frictions of cargo hoisting as well as the trolley and bridge motions are linearly characterized by damping coefficients b_r, b_t, and b_b, respectively. The control signals u_b, u_t, and u_l correspondingly demonstrate the driving forces of the trolley motion, bridge movement, and cargo lifting translation.

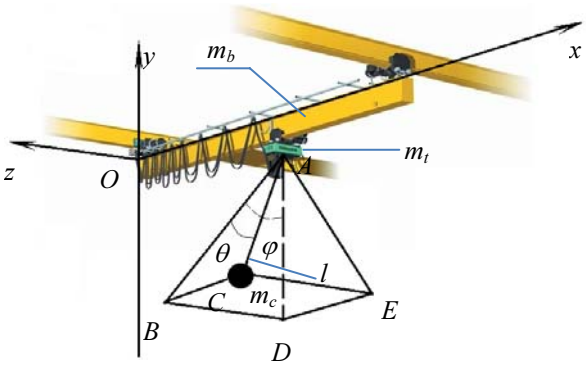

Fig. 1. Physical modeling of a 3D overhead crane.

Using Lagrange's equation, Lee [35] proposed the dynamics of the overhead crane composed of five nonlinear ordinary differential equations as follows:

$$\left.\begin{aligned}&(m_t+m_b+m_c)\ddot{z}+m_c\sin\varphi\cos\theta\ddot{l}\\&+m_c l\cos\varphi\cos\theta\ddot{\varphi}-m_c l\sin\varphi\sin\theta\ddot{\theta}\\&+b_b\dot{z}+2m_c\cos\varphi\cos\theta\dot{l}\dot{\varphi}\\&-2m_c\sin\varphi\sin\theta\dot{l}\dot{\theta}-2m_c l\cos\varphi\sin\theta\dot{\varphi}\dot{\theta}\\&-m_c l\sin\varphi\cos\theta\dot{\varphi}^2-m_c l\sin\varphi\cos\theta\dot{\theta}^2\end{aligned}\right]=u_b, \tag{1}$$

$$\left.\begin{aligned}&(m_t+m_c)\ddot{x}+m_c\sin\theta\ddot{l}+m_c l\cos\theta\ddot{\theta}\\&+b_t\dot{x}+2m_c\cos\theta\dot{l}\dot{\theta}-m_c l\sin\theta\dot{\theta}^2\end{aligned}\right]=u_t, \tag{2}$$

$$\left.\begin{aligned}&(m_l+m_c)\ddot{l}+m_c\sin\theta\ddot{x}+m_c\sin\varphi\cos\theta\ddot{z}\\&+b_r\dot{l}-m_c l\dot{\theta}^2-m_c l\cos^2\theta\dot{\varphi}^2-m_c g\cos\varphi\cos\theta\end{aligned}\right]=u_l, \tag{3}$$

$$\left.\begin{aligned}&m_c l\cos\varphi\cos\theta\ddot{z}+m_c l^2\cos^2\theta\ddot{\varphi}+2m_c l\cos^2\theta\dot{l}\dot{\varphi}\\&-2m_c l^2\cos\theta\sin\theta\dot{\varphi}\dot{\theta}+m_c gl\sin\varphi\cos\theta\end{aligned}\right]=0, \tag{4}$$

$$\left.\begin{aligned}&m_c l\cos\theta\ddot{x}-m_c l\sin\varphi\sin\theta\ddot{z}+m_c l^2\ddot{\theta}\\&+2m_c l\dot{l}\dot{\theta}+m_c l^2\cos\theta\sin\theta\dot{\varphi}^2+m_c gl\cos\varphi\sin\theta\end{aligned}\right]=0. \tag{5}$$

The aforementioned system dynamics can be represented in matrix form as

$$\mathbf{M}(\mathbf{q})\ddot{\mathbf{q}}+\mathbf{B}\dot{\mathbf{q}}+\mathbf{C}(\mathbf{q},\dot{\mathbf{q}})\dot{\mathbf{q}}+\mathbf{G}(\mathbf{q})=\mathbf{F}. \tag{6}$$

where $\mathbf{M}(\mathbf{q})=\mathbf{M}^T(\mathbf{q})$ is the symmetric mass matrix, $\mathbf{B}$ is the damping coefficient matrix, $\mathbf{C}(\mathbf{q},\dot{\mathbf{q}})$ is the Coriolis

and centrifugal matrix, $\mathbf{G}(\mathbf{q})$ indicates a gravity matrix, and $\mathbf{F}$ denotes the matrix of the control forces of the driving motors. These matrixes are determined by the following formulas:

$$\mathbf{G}(\mathbf{q})=\begin{bmatrix}0\\0\\g_3\\g_4\\g_5\end{bmatrix},\ \mathbf{M}(\mathbf{q})=\begin{bmatrix}m_{11}&0&m_{13}&m_{14}&m_{15}\\0&m_{22}&m_{23}&0&m_{25}\\m_{31}&m_{32}&m_{33}&0&0\\m_{41}&0&0&m_{44}&0\\m_{51}&m_{52}&0&0&m_{55}\end{bmatrix},$$

$$\mathbf{F}=\begin{bmatrix}u_b\\u_t\\u_l\\0\\0\end{bmatrix},\quad \mathbf{q}=\begin{bmatrix}z\\x\\l\\\varphi\\\theta\end{bmatrix},\quad \mathbf{B}=\begin{bmatrix}b_b&0&0&0&0\\0&b_t&0&0&0\\0&0&b_r&0&0\\0&0&0&0&0\\0&0&0&0&0\end{bmatrix},$$

$$\mathbf{C}(\mathbf{q},\dot{\mathbf{q}})=\begin{bmatrix}0&0&c_{13}&c_{14}&c_{15}\\0&0&c_{23}&0&c_{25}\\0&0&0&c_{34}&c_{35}\\0&0&c_{43}&c_{44}&c_{45}\\0&0&c_{53}&c_{54}&c_{55}\end{bmatrix}.$$

The coefficients of the $\mathbf{M}(\mathbf{q})$ matrix are given by

$$m_{11}=m_t+m_b+m_c,\quad m_{13}=m_{31}=m_c\sin\varphi\cos\theta,$$
$$m_{14}=m_{41}=m_c l\cos\varphi\cos\theta,$$
$$m_{15}=m_{51}=-m_c l\sin\varphi\sin\theta,\quad m_{22}=m_t+m_c,$$
$$m_{23}=m_c\sin\theta,\quad m_{25}=m_{52}=m_c l\cos\theta,$$
$$m_{32}=m_c\sin\theta,\quad m_{33}=m_l+m_c,$$
$$m_{44}=m_c l^2\cos^2\theta,\quad m_{55}=m_c l^2.$$

The coefficients of the $\mathbf{C}(\mathbf{q},\dot{\mathbf{q}})$ matrix are determined by

$$c_{13}=m_c\cos\varphi\cos\theta\dot{\varphi}-m_c\sin\varphi\sin\theta\dot{\theta},$$
$$c_{14}=m_c\cos\varphi\cos\theta\dot{l}-m_c l\cos\varphi\sin\theta\dot{\theta}-m_c l\sin\varphi\cos\theta\dot{\varphi},$$
$$c_{15}=-m_c l\cos\varphi\sin\theta\dot{\varphi}-m_c\sin\varphi\sin\theta\dot{l}-m_c l\sin\varphi\cos\theta\dot{\theta},$$
$$c_{23}=m_c\cos\theta\dot{\theta},\quad c_{25}=m_c\cos\theta\dot{l}-m_c l\sin\theta\dot{\theta},$$
$$c_{34}=-m_c l\cos^2\theta\dot{\varphi},\quad c_{35}=-m_c l\dot{\theta},\quad c_{43}=m_c l\cos^2\theta\dot{\varphi},$$
$$c_{44}=m_c l\cos^2\theta\dot{l}-m_c l^2\cos\theta\sin\theta\dot{\theta},$$
$$c_{45}=-m_c l^2\cos\theta\sin\theta\dot{\varphi},\quad c_{53}=m_c l\dot{\theta},$$
$$c_{54}=m_c l^2\cos\theta\sin\theta\dot{\varphi},\quad c_{55}=m_c l\dot{l}.$$

The nonzero coefficients of the $\mathbf{G}(\mathbf{q})$ vector are given by

$$g_3=-m_c g\cos\varphi\cos\theta,\quad g_4=m_c gl\sin\varphi\cos\theta,$$
$$g_5=m_c gl\cos\varphi\sin\theta.$$

3. CONTROL SCHEME DESIGN

3.1. Decoupling

The overhead crane is an under-actuated system in which five output signals are driven by three actuators. Its mathematical model should be separated into two auxiliary system dynamics, namely, actuated and un-actuated systems. Correspondingly, $\mathbf{q}_1=[z\quad x\quad l]^T$ for actuated states and $\mathbf{q}_2=[\varphi\quad\theta]^T$ for un-actuated states are defined. The matrix differential equation (6) can then be divided into two equations as follows:

$$\begin{pmatrix}\mathbf{M}_{11}(\mathbf{q})\ddot{\mathbf{q}}_1+\mathbf{M}_{12}(\mathbf{q})\ddot{\mathbf{q}}_2+\mathbf{B}_{11}\dot{\mathbf{q}}_1\\+\mathbf{C}_{11}(\mathbf{q},\dot{\mathbf{q}})\dot{\mathbf{q}}_1+\mathbf{C}_{12}(\mathbf{q},\dot{\mathbf{q}})\dot{\mathbf{q}}_2+\mathbf{G}_1(\mathbf{q})\end{pmatrix}=\mathbf{U},\tag{7}$$

$$\begin{pmatrix}\mathbf{M}_{21}(\mathbf{q})\ddot{\mathbf{q}}_1+\mathbf{M}_{22}(\mathbf{q})\ddot{\mathbf{q}}_2+\mathbf{C}_{21}(\mathbf{q},\dot{\mathbf{q}})\dot{\mathbf{q}}_1\\+\mathbf{C}_{22}(\mathbf{q},\dot{\mathbf{q}})\dot{\mathbf{q}}_2+\mathbf{G}_2(\mathbf{q})\end{pmatrix}=\mathbf{0},\tag{8}$$

where

$$\mathbf{M}_{11}(\mathbf{q})=\begin{bmatrix}m_{11}&0&m_{13}\\0&m_{22}&m_{23}\\m_{31}&m_{32}&m_{33}\end{bmatrix},\ \mathbf{M}_{12}(\mathbf{q})=\begin{bmatrix}m_{14}&m_{15}\\0&m_{25}\\0&0\end{bmatrix},$$
$$\mathbf{M}_{21}(\mathbf{q})=\begin{bmatrix}m_{41}&0&0\\m_{51}&m_{52}&0\end{bmatrix},\ \mathbf{M}_{22}(\mathbf{q})=\begin{bmatrix}m_{44}&0\\0&m_{55}\end{bmatrix},$$
$$\mathbf{C}_{11}(\mathbf{q},\dot{\mathbf{q}})=\begin{bmatrix}0&0&c_{13}\\0&0&c_{23}\\0&0&0\end{bmatrix},\quad \mathbf{C}_{12}(\mathbf{q},\dot{\mathbf{q}})=\begin{bmatrix}c_{14}&c_{15}\\0&c_{25}\\c_{34}&c_{35}\end{bmatrix},$$
$$\mathbf{C}_{21}(\mathbf{q},\dot{\mathbf{q}})=\begin{bmatrix}0&0&c_{43}\\0&0&c_{53}\end{bmatrix},\quad \mathbf{C}_{22}(\mathbf{q},\dot{\mathbf{q}})=\begin{bmatrix}c_{44}&c_{45}\\c_{54}&c_{55}\end{bmatrix},$$
$$\mathbf{B}_{11}=\begin{bmatrix}b_t&0&0\\0&b_b&0\\0&0&b_r\end{bmatrix},\ \mathbf{G}_1=\begin{bmatrix}0\\0\\g_3\end{bmatrix},\ \mathbf{G}_2=\begin{bmatrix}g_4\\g_5\end{bmatrix},\ \mathbf{U}=\begin{bmatrix}u_b\\u_t\\u_l\end{bmatrix}.$$

Therefore, matrices $\mathbf{M}(\mathbf{q})$ and $\mathbf{C}(\mathbf{q},\dot{\mathbf{q}})$ of (6) have the following form:

$$\mathbf{M}(\mathbf{q})=\begin{bmatrix}\mathbf{M}_{11}(\mathbf{q})&\mathbf{M}_{12}(\mathbf{q})\\\mathbf{M}_{21}(\mathbf{q})&\mathbf{M}_{22}(\mathbf{q})\end{bmatrix},$$
$$\mathbf{C}(\mathbf{q},\dot{\mathbf{q}})=\begin{bmatrix}\mathbf{C}_{11}(\mathbf{q},\dot{\mathbf{q}})&\mathbf{C}_{12}(\mathbf{q},\dot{\mathbf{q}})\\\mathbf{C}_{21}(\mathbf{q},\dot{\mathbf{q}})&\mathbf{C}_{22}(\mathbf{q},\dot{\mathbf{q}})\end{bmatrix}.$$

The actuated equation (7) shows the direct constraint between the actuated states $\mathbf{q}_1$ and the actuators $\mathbf{U}$. However, the un-actuated equation (8) does not display the relationship between the un-actuated states $\mathbf{q}_2$ and the inputs $\mathbf{U}$. Physically, the input signals $\mathbf{U}$ directly control the actuated states $\mathbf{q}_1$ and indirectly drive the un-actuated states $\mathbf{q}_2$.

3.2. Partial feedback Linearization

The dynamics of the closed-loop system comprising (7) and (8) is transferred into an equivalent linear form based on the nonlinear feedback technique. Note that $\mathbf{M}_{22}(\mathbf{q})$ is a positive definite matrix for every $l>0$ and $|\theta|<\pi/2$. The un-actuated states $\mathbf{q}_2$ can be determined from (8) as

$$\ddot{\mathbf{q}}_2=-\mathbf{M}_{22}^{-1}(\mathbf{q})\begin{pmatrix}\mathbf{M}_{21}(\mathbf{q})\ddot{\mathbf{q}}_1+\mathbf{C}_{21}(\mathbf{q},\dot{\mathbf{q}})\dot{\mathbf{q}}_1\\+\mathbf{C}_{22}(\mathbf{q},\dot{\mathbf{q}})\dot{\mathbf{q}}_2+\mathbf{G}_2(\mathbf{q})\end{pmatrix}.\tag{9}$$

Observe that the cargo swing $\mathbf{q}_2=[\varphi\quad\theta]^T$ is directly

related to the properties of the trolley motion x, bridge motion z, and the length of the wire rope l. Substituting (9) into (7) and simplifying the equation lead to the following:

$$\bar{\mathbf{M}}(\mathbf{q})\ddot{\mathbf{q}}_1 + \bar{\mathbf{C}}_1(\mathbf{q},\dot{\mathbf{q}})\dot{\mathbf{q}}_1 + \bar{\mathbf{C}}_2(\mathbf{q},\dot{\mathbf{q}})\dot{\mathbf{q}}_2 + \bar{\mathbf{G}}(\mathbf{q}) = \mathbf{U}, \quad (10)$$

where

$$\bar{\mathbf{M}}(\mathbf{q}) = \mathbf{M}_{11}(\mathbf{q}) - \mathbf{M}_{12}(\mathbf{q})\mathbf{M}_{22}^{-1}(\mathbf{q})\mathbf{M}_{21}(\mathbf{q}),$$
$$\bar{\mathbf{C}}_1(\mathbf{q},\dot{\mathbf{q}}) = \mathbf{B}_{11} + \mathbf{C}_{11}(\mathbf{q},\dot{\mathbf{q}}) - \mathbf{M}_{12}(\mathbf{q})\mathbf{M}_{22}^{-1}(\mathbf{q})\mathbf{C}_{21}(\mathbf{q},\dot{\mathbf{q}}),$$
$$\bar{\mathbf{C}}_2(\mathbf{q},\dot{\mathbf{q}}) = \mathbf{C}_{12}(\mathbf{q},\dot{\mathbf{q}}) - \mathbf{M}_{12}(\mathbf{q})\mathbf{M}_{22}^{-1}(\mathbf{q})\mathbf{C}_{22}(\mathbf{q},\dot{\mathbf{q}}),$$
$$\bar{\mathbf{G}}(\mathbf{q}) = \mathbf{G}_1(\mathbf{q}) - \mathbf{M}_{12}(\mathbf{q})\mathbf{M}_{22}^{-1}(\mathbf{q})\mathbf{G}_2(\mathbf{q}).$$

Note that matrix $\bar{\mathbf{M}}(\mathbf{q})$ is positive definite for every $l > 0$, $|\varphi| < \pi/2$, and $|\theta| < \pi/2$. Equation (10) can be represented as

$$\ddot{\mathbf{q}}_1 = \bar{\mathbf{M}}^{-1}(\mathbf{q})\left(\mathbf{U} - \bar{\mathbf{C}}_1(\mathbf{q},\dot{\mathbf{q}})\dot{\mathbf{q}}_1 - \bar{\mathbf{C}}_2(\mathbf{q},\dot{\mathbf{q}})\dot{\mathbf{q}}_2 - \bar{\mathbf{G}}(\mathbf{q})\right). \quad (11)$$

Substituting (11) into (9) yields

$$\ddot{\mathbf{q}}_2 = -\mathbf{M}_{22}^{-1}(\mathbf{q})\left(\begin{array}{l}\mathbf{M}_{21}(\mathbf{q})\bar{\mathbf{M}}^{-1}(\mathbf{q})\begin{pmatrix}\mathbf{U} - \bar{\mathbf{C}}_1(\mathbf{q},\dot{\mathbf{q}})\dot{\mathbf{q}}_1 \\ -\bar{\mathbf{C}}_2(\mathbf{q},\dot{\mathbf{q}})\dot{\mathbf{q}}_2 - \bar{\mathbf{G}}(\mathbf{q})\end{pmatrix} \\ +\mathbf{C}_{21}(\mathbf{q},\dot{\mathbf{q}})\dot{\mathbf{q}}_1 + \mathbf{C}_{22}(\mathbf{q},\dot{\mathbf{q}})\dot{\mathbf{q}}_2 + \mathbf{G}_2(\mathbf{q})\end{array}\right). \quad (12)$$

Therefore, the physical behavior of the crane system can be characterized by actuated (11) and un-actuated dynamics (12) in which the mathematical relationships between $\mathbf{q}_1$, $\mathbf{q}_2$, and $\mathbf{U}$ can be observed clearly.

Considering the actuated states $\mathbf{q}_1$ as the system outputs, the actuated dynamics can be "linearized" (11) by defining

$$\ddot{\mathbf{q}}_1 = \mathbf{V}_a \quad (13)$$

with $\mathbf{V}_a \in \mathbf{R}^3$ as the equivalent control inputs. Then, the control signals $\mathbf{U}$ become

$$\mathbf{U} = \bar{\mathbf{M}}(\mathbf{q})\mathbf{V}_a + \bar{\mathbf{C}}_1(\mathbf{q},\dot{\mathbf{q}})\dot{\mathbf{q}}_1 + \bar{\mathbf{C}}_2(\mathbf{q},\dot{\mathbf{q}})\dot{\mathbf{q}}_2 + \bar{\mathbf{G}}(\mathbf{q}). \quad (14)$$

The controller $\mathbf{U}$ is designed to drive the actuated states $\mathbf{q}_1 = [z \quad x \quad l]^T$ to the desired constant values $\mathbf{q}_{1d} = [z_d \quad x_d \quad l_d]^T$. To track the given state trajectories, the following equivalent control inputs are chosen:

$$\mathbf{V}_a = \ddot{\mathbf{q}}_{1d} - \mathbf{K}_{ad}(\dot{\mathbf{q}}_1 - \dot{\mathbf{q}}_{1d}) - \mathbf{K}_{ap}(\mathbf{q}_1 - \mathbf{q}_{1d}). \quad (15)$$

As $\mathbf{q}_{1d}$ = **const**, (15) can be reduced as

$$\mathbf{V}_a = -\mathbf{K}_{ad}\dot{\mathbf{q}}_1 - \mathbf{K}_{ap}(\mathbf{q}_1 - \mathbf{q}_{1d}) \quad (16)$$

with $\mathbf{K}_{ad} = \mathrm{diag}(K_{ad1}, K_{ad2}, K_{ad3})$, $\mathbf{K}_{ap} = \mathrm{diag}(K_{ap1}, K_{ap2}, K_{ap3})$ as positive diagonal matrices.

Referring to (15) and to active dynamics (13), the differential equation of the tracking error is obtained as described by

$$\ddot{\tilde{\mathbf{q}}}_1 + \mathbf{K}_{ad}\dot{\tilde{\mathbf{q}}}_1 + \mathbf{K}_{ap}\tilde{\mathbf{q}}_1 = \mathbf{0}, \quad (17)$$

where $\tilde{\mathbf{q}}_1 = \mathbf{q}_1 - \mathbf{q}_{1d}$ is the tracking error vector of the actuated states. Clearly, the dynamics of the tracking error (17) is exponentially stable for every $\mathbf{K}_{ad} > \mathbf{0}$ and $\mathbf{K}_{ap} > \mathbf{0}$ (with the initial condition $\tilde{\mathbf{q}}_1(0) = \mathbf{0}$, $\tilde{\mathbf{q}}_1(t) \equiv \mathbf{0}$ $\forall t > 0$). In other words, the tracking errors of the actuated states $\tilde{\mathbf{q}}_1$ approach zeros (or $\mathbf{q}_1$ converges to $\mathbf{q}_{1d}$) as t becomes infinite. More precisely, the equivalent control $\mathbf{V}_a$ forces the actuated states $\mathbf{q}_1$ to reach the references $\mathbf{q}_{1d}$ asymptotically.

The control scheme (14) corresponding to the equivalent input $\mathbf{V}_a$ is only used for asymptotically stabilizing the actuated states $\mathbf{q}_1$. To stabilize un-actuated states $\mathbf{q}_2$, the nonlinear feedback method can be applied to the sub-dynamics (12) as follows:

$$\ddot{\mathbf{q}}_2 = \mathbf{V}_u = -\mathbf{K}_{ud}\dot{\mathbf{q}}_2 - \mathbf{K}_{up}\mathbf{q}_2, \quad (18)$$

where $\mathbf{V}_u \in \mathbf{R}^2$ are the equivalent inputs of the un-actuated states. $\mathbf{K}_{ud} = \mathrm{diag}(K_{ud1}, K_{ud2})$ and $\mathbf{K}_{up} = \mathrm{diag}(K_{up1}, K_{up2})$ are positive matrices. The control input $\mathbf{U}$ received from (12) and (18) ensures the stability of the un-actuated states $\mathbf{q}_2$ because the tracking error dynamics

$$\ddot{\mathbf{q}}_2 + \mathbf{K}_{ud}\dot{\mathbf{q}}_2 + \mathbf{K}_{up}\mathbf{q}_2 = \mathbf{0} \quad (19)$$

is stable for every $\mathbf{K}_{ud} > \mathbf{0}$ and $\mathbf{K}_{up} > \mathbf{0}$. In other words, if $\mathbf{K}_{ud}$ and $\mathbf{K}_{up}$ are selected properly, the equivalent inputs $\mathbf{V}_u$ drive the cargo swings $\mathbf{q}_2 = [\varphi \quad \theta]^T$ toward to zeros.

For stabilizing the un-actuated and actuated states, the overall equivalent inputs are proposed by linearly combining $\mathbf{V}_a$ and $\mathbf{V}_u$ as follows:

$$\begin{aligned}\mathbf{V} &= \mathbf{V}_a + \boldsymbol{\alpha}\mathbf{V}_u \\ &= -\mathbf{K}_{ad}\dot{\mathbf{q}}_1 - \mathbf{K}_{ap}(\mathbf{q}_1 - \mathbf{q}_{1d}) - \boldsymbol{\alpha}(\mathbf{K}_{ud}\dot{\mathbf{q}}_2 + \mathbf{K}_{up}\mathbf{q}_2)\end{aligned} \quad (20)$$

with $\boldsymbol{\alpha} = \begin{bmatrix}\alpha_1 & 0 \\ 0 & \alpha_2 \\ 0 & 0\end{bmatrix}$ as a weighting matrix and $\mathbf{V} \in \mathbf{R}^3$.

Hence, considering $\mathbf{q}_1$ as the primary output, the total control scheme is determined by replacing $\mathbf{V}_a$ with $\mathbf{V}$ in (14). Substituting (20) into (14), the PFL control structure is obtained as

$$\begin{aligned}\mathbf{U} = &\left(\bar{\mathbf{C}}_1(\mathbf{q},\dot{\mathbf{q}}) - \bar{\mathbf{M}}(\mathbf{q})\mathbf{K}_{ad}\right)\dot{\mathbf{q}}_1 \\ &+ \left(\bar{\mathbf{C}}_2(\mathbf{q},\dot{\mathbf{q}}) - \bar{\mathbf{M}}(\mathbf{q})\boldsymbol{\alpha}\mathbf{K}_{ud}\right)\dot{\mathbf{q}}_2 \\ &- \bar{\mathbf{M}}(\mathbf{q})\mathbf{K}_{ap}(\mathbf{q}_1 - \mathbf{q}_{1d}) \\ &- \bar{\mathbf{M}}(\mathbf{q})\boldsymbol{\alpha}\mathbf{K}_{up}\mathbf{q}_2 + \bar{\mathbf{G}}(\mathbf{q}).\end{aligned} \quad (21)$$

As seen in the simulation and experiment section, the nonlinear controller (21) asymptotically stabilizes all system state trajectories.

3.3. System stability

The control law $\mathbf{U}$ is referred from the actuated dynamics (11). The stability of the remaining part (un-actuated part) of the closed-loop system called internal

dynamics is analyzed. If the internal dynamics is stable, then the tracking control problem is solved. Substituting the control scheme (21) into the un-actuated subsystem (12) yields the internal dynamics.

$$\ddot{\mathbf{q}}_2 = -\mathbf{M}_{22}^{-1}(\mathbf{q})\begin{pmatrix} -\mathbf{M}_{21}(\mathbf{q})\begin{pmatrix} \mathbf{K}_{ad}\dot{\mathbf{q}}_1 + \boldsymbol{\alpha}\mathbf{K}_{ud}\dot{\mathbf{q}}_2 \\ +\mathbf{K}_{ap}(\mathbf{q}_1 - \mathbf{q}_{1d}) + \boldsymbol{\alpha}\mathbf{K}_{up}\mathbf{q}_2 \end{pmatrix} \\ +\mathbf{C}_{21}(\mathbf{q},\dot{\mathbf{q}})\dot{\mathbf{q}}_1 + \mathbf{C}_{22}(\mathbf{q},\dot{\mathbf{q}})\dot{\mathbf{q}}_2 + \mathbf{G}_2(\mathbf{q}) \end{pmatrix}. \tag{22}$$

The local stability of the internal dynamics is guaranteed if the zero dynamics is exponentially stable. Setting $\mathbf{q}_1 = \mathbf{q}_{1d}$ in the internal dynamics (22), the zero dynamics of the system is obtained as

$$\ddot{\mathbf{q}}_2 + \mathbf{M}_{22}^{-1}(\mathbf{q})\begin{pmatrix} \left(\mathbf{C}_{22}(\mathbf{q},\dot{\mathbf{q}}) - \mathbf{M}_{21}(\mathbf{q})\boldsymbol{\alpha}\mathbf{K}_{ud}\right)\dot{\mathbf{q}}_2 \\ -\mathbf{M}_{21}(\mathbf{q})\boldsymbol{\alpha}\mathbf{K}_{up}\mathbf{q}_2 + \mathbf{G}_2(\mathbf{q}) \end{pmatrix} = \mathbf{0}, \tag{23}$$

which is expanded into two expressions as

$$\begin{pmatrix} l_d\ddot{\varphi} - 2l_d\tan\theta\dot{\theta}\dot{\varphi} - \alpha_1 K_{ud1}\dfrac{\cos\varphi}{\cos\theta}\dot{\varphi} \\ -\alpha_1 K_{up1}\dfrac{\cos\varphi}{\cos\theta}\varphi + g\dfrac{\sin\varphi}{\cos\theta} \end{pmatrix} = 0, \tag{24}$$

$$\begin{pmatrix} l_d\ddot{\theta} + l_d\cos\theta\sin\theta\dot{\varphi}^2 + \alpha_1 K_{ud1}\sin\varphi\sin\theta\dot{\varphi} \\ -\alpha_2 K_{ud2}\cos\theta\dot{\theta} + \alpha_1 K_{up1}\sin\varphi\sin\theta\varphi \\ -\alpha_2 K_{up2}\cos\theta\theta + g\cos\varphi\sin\theta \end{pmatrix} = 0. \tag{25}$$

The stability of the zero dynamics comprising (24) and (25) is analyzed using the Lyapunov's linearization theorem. First, we represent the zero dynamics in the first-order form by setting four state variables as

$$z_1 = \varphi, \quad z_2 = \dot{\varphi}, \quad z_3 = \theta, \quad z_4 = \dot{\theta}.$$

Then, the zero-dynamics is of the following state-space forms:

$$\dot{z}_1 = z_2, \tag{26}$$

$$\dot{z}_2 = \begin{pmatrix} 2\tan z_3 z_4 z_2 + \dfrac{\alpha_1 K_{ud1}}{l_d}\dfrac{\cos z_1}{\cos z_3}z_2 \\ +\dfrac{\alpha_1 K_{up1}}{l_d}\dfrac{\cos z_1}{\cos z_3}z_1 - \dfrac{g}{l_d}\dfrac{\sin z_1}{\cos z_3} \end{pmatrix} = f(\mathbf{z}), \tag{27}$$

$$\dot{z}_3 = z_4, \tag{28}$$

$$\dot{z}_4 = \begin{pmatrix} -\cos z_3\sin z_3 z_2^2 - \dfrac{\alpha_1 K_{ud1}}{l_d}\sin z_1\sin z_3 z_2 \\ \dfrac{\alpha_2 K_{ud2}}{l_d}\cos z_3 z_4 - \dfrac{\alpha_1 K_{up1}}{l_d}\sin z_1\sin z_3 z_1 \\ \dfrac{\alpha_2 K_{up2}}{l_d}\cos z_3 z_3 - \dfrac{g}{l_d}\cos z_1\sin z_3 \end{pmatrix} = g(\mathbf{z}) \tag{29}$$

with $\mathbf{z} = [z_1 \;\; z_2 \;\; z_3 \;\; z_4]^T$ as a state vector. The nonlinear zero dynamics (26)-(29) is asymptotically stable around the equilibrium point $\mathbf{z} = \mathbf{0}\,(\mathbf{q}_2 = \dot{\mathbf{q}}_2 = \mathbf{0})$ if the corresponding linearized system is strictly stable. Linearizing the zero dynamics around $\mathbf{z} = \mathbf{0}$ yields a linearized system in the following form:

$$\dot{\mathbf{z}} = \mathbf{A}\mathbf{z}, \tag{30}$$

where

$$\mathbf{A} = \begin{bmatrix} 0 & 1 & 0 & 0 \\ \dfrac{\partial f}{\partial z_1} & \dfrac{\partial f}{\partial z_2} & \dfrac{\partial f}{\partial z_3} & \dfrac{\partial f}{\partial z_4} \\ 0 & 0 & 0 & 1 \\ \dfrac{\partial g}{\partial z_1} & \dfrac{\partial g}{\partial z_2} & \dfrac{\partial g}{\partial z_3} & \dfrac{\partial g}{\partial z_4} \end{bmatrix}_{\mathbf{z}=\mathbf{0}} = \begin{bmatrix} 0 & 1 & 0 & 0 \\ \dfrac{\alpha_1 K_{up1} - g}{l_d} & \dfrac{\alpha_1 K_{ud1}}{l_d} & 0 & 0 \\ 0 & 0 & 0 & 1 \\ 0 & 0 & -\dfrac{g}{l_d} & \dfrac{\alpha_2 K_{ud2}}{l_d} \end{bmatrix} \tag{31}$$

is a Jacobian matrix whose characteristic polynomial has the following form:

$$\begin{aligned} \left|\mathbf{A} - s\mathbf{I}_4\right| = s^4 &- \left(\frac{K_{ud1}\alpha_1 + K_{ud2}\alpha_2}{l_d}\right)s^3 \\ &+ \left(\frac{2g - K_{up1}\alpha_1}{l_d} + \frac{K_{ud1}K_{ud2}\alpha_1\alpha_2}{l_d^2}\right)s^2 \\ &- \frac{K_{ud1}\alpha_1 g + K_{ud2}\alpha_2\left(g - K_{up1}\alpha_1\right)}{l_d^2}s \\ &+ \frac{g\left(g - K_{up1}\alpha_1\right)}{l_d^2}. \end{aligned} \tag{32}$$

The linearized system (30) is stable around the equilibrium point $\mathbf{z} = \mathbf{0}$ if $\mathbf{A}$ is a Hurwitz matrix. Based on Hurwitz's criterion and the results of the calculations, the constraint condition of the controller parameters is determined as

$$(K_{ud1}\alpha_1 + K_{ud2}\alpha_2) < 0, \tag{33a}$$

$$l_d(K_{up1}\alpha_1 - 2g) < K_{ud1}K_{ud2}\alpha_1\alpha_2, \tag{33b}$$

$$K_{ud1}\alpha_1 g < K_{ud2}\alpha_2(K_{up1}\alpha_1 - g), \tag{33c}$$

$$K_{up1}\alpha_1 < g. \tag{33d}$$

Therefore, if the relationships (33) among control parameters are held, the zero dynamics is stable around equilibrium point $\mathbf{z} = \mathbf{0}$, which leads to the local stability of the internal dynamics (22).

4. SIMULATION AND REAL-TIME EXPERIMENT

The overhead crane dynamics (6) driven by control inputs (21) is numerically simulated in the case of a crane system involving complicated operations. Accord-

Table 1. Crane system parameters.

System dynamics	Controller
$g = 9.81$ m/s^2, $m_c = 0.85$ kg, $m_t = 5$ kg, $m_b = 7$ kg, $m_l = 2$ kg, $b_t = 20$ N.m/s, $b_b = 30$ Nm/s, $b_r = 50$ Nm/s	$\mathbf{K}_{ad} = \text{diag}(1.5,1.5,2.5)$ $\mathbf{K}_{ud} = \text{diag}(3,3)$ $\mathbf{K}_{ap} = \text{diag}(0.85,0.87,2)$ $\mathbf{K}_{up} = \text{diag}(0.5,0.5)$ $\alpha_1 = \alpha_2 = -1$

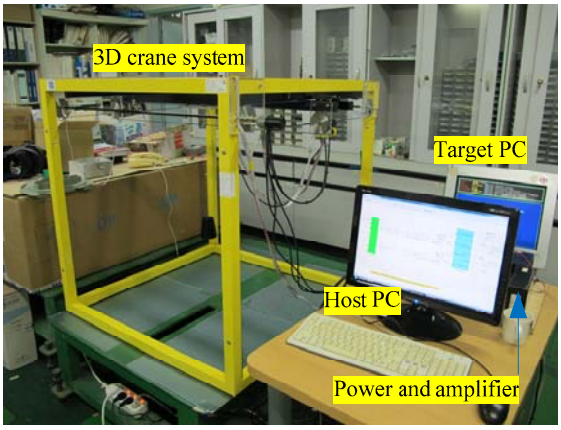

Fig. 2. An overhead crane system for the experiments.

ingly, the trolley is forced to move from its initial position to the desired displacement at 0.4 m, the bridge is driven from its starting point to the desired location at 0.3 m, and the cargo is lifted with a cable length of 1 m to 0.7 m of cable reference. These processes (lifting the cargo, moving the trolley, travelling the bridge) must be initiated at the same time, with the cargo suspension cable initially perpendicular to the ground. The parameters used for the simulation are given on Table 1.

Furthermore, an experimental study is employed to clarify the simulation results. The overhead crane system used for the experiment is shown in Fig. 2. This system uses three DC motors for the bridge travelling, trolley moving, and cargo hoisting functions. Five incremental encoders are used to measure the bridge and trolley displacements, the transportation of cargo along the cable, and the swing angles of the two payloads.

The real-time system is controlled by a target PC in which a controller is designed based on MATLAB/ SIMULINK environment with an xPC target solution. Accordingly, a host PC is connected to the target PC, and the crane system is linked to the target PC by two interface cards. The real-time system is controlled by a target PC in which a controller is designed based on MATLAB/SIMULINK environment with an xPC target solution. Accordingly, a host PC is connected to the target PC, and the crane system is linked to the target PC by two interface cards. The NI PCI 6602 card sends PWM signals to the motor amplifiers and acquires feedback pulses from the encoders. The NI PCI 6025E multifunction card is used to send the direction control signals to the motor amplifiers.

The results in both the simulation and the experiment are illustrated in Figs. 3-15. Figs. 3-5 describe the paths

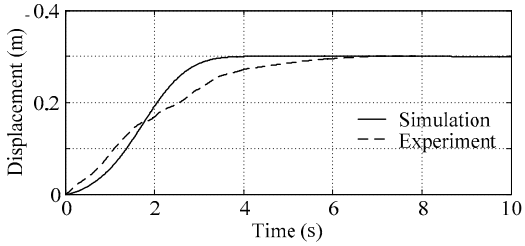

Fig. 3. Bridge motion.

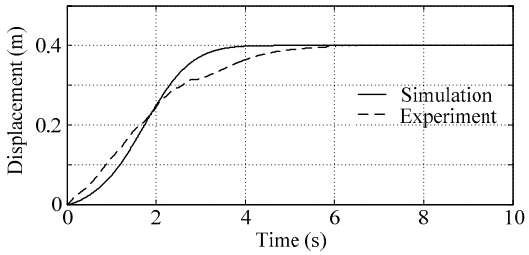

Fig. 4. Trolley motion.

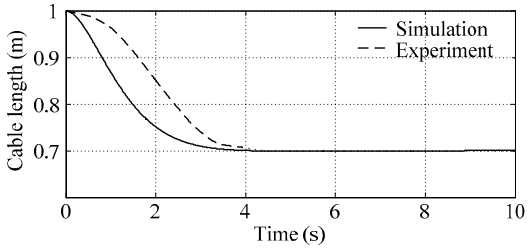

Fig. 5. Cargo hoisting motion.

of the bridge motion, trolley movement, and the payload lifting translation. All trajectories asymptotically converge to the references. However, the simulation curves are smoother and achieve steady states earlier than those in Experiment 1. The bridge moves and stops accurately at the load endpoint after 4 seconds for the simulation and 6 seconds for the experiment. The trolley reaches its destination after 4.1 seconds for the simulation and 6.2 for the experiment. The cargo is lifted from an initial cable length of 1 m to the desired cable length at 0.7 m after 4.2 seconds for both the simulation and the experiment.

The responses of the cargo swings are depicted in Figs. 6-7. The cargo swings are bounded with small angles during the cargo transfer process—$\varphi_{\max} = 2.2°$ and $\theta_{\max} = 2.9°$ for the simulation and $\varphi_{\max} = 2.3°$ and $\theta_{\max} = 2.4°$ for the experiment. The simulated cargo swings are entirely suppressed after the short settling times, namely, $t_s = 4$ s for φ and $t_s = 4.5$ s for θ, within one vibration period. Tiny steady-state errors remain in the experimental responses, which reach the approximate steady-state after over two oscillation periods.

The velocities of the system responses shown in Figs. 8-12 asymptotically reach zeros. The motions of the bridge and trolley as well as the lifting movement of the payload at transient states are composed of two stages: the increasing and decreasing velocity periods. As seen clear in the simulated curves, the trolley speeds up within

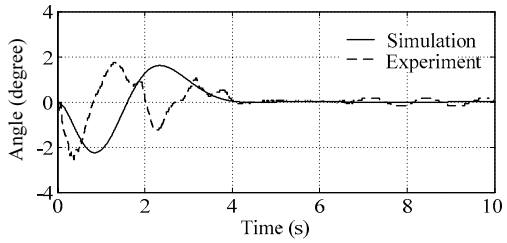

Fig. 6. Cargo swing angle φ.

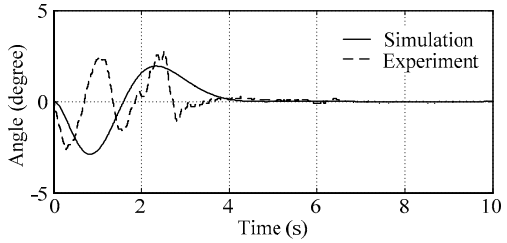

Fig. 7. Cargo swing angle θ.

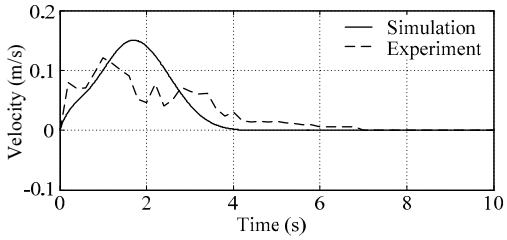

Fig. 8. Velocity of bridge motion.

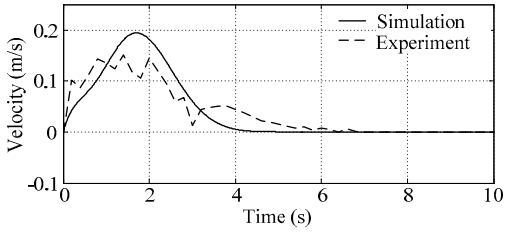

Fig. 9. Velocity of trolley motion.

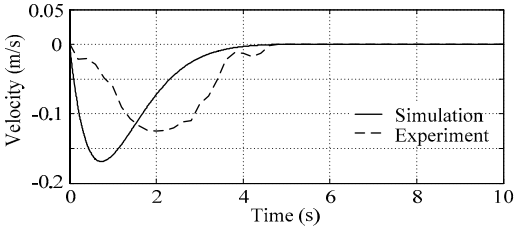

Fig. 10. Cargo hoisting velocity.

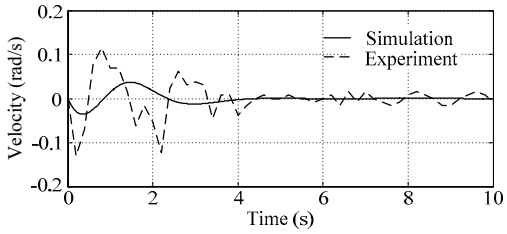

Fig. 11. Payload swing velocity $\dot{\varphi}$.

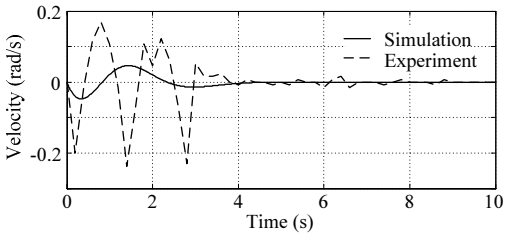

Fig. 12. Payload swing velocity $\dot{\theta}$.

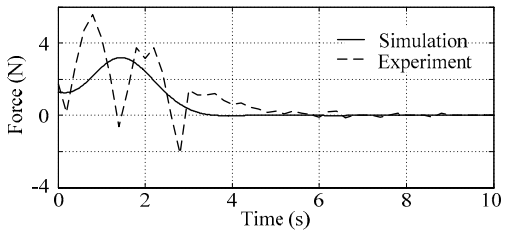

Fig. 13. Bridge moving force.

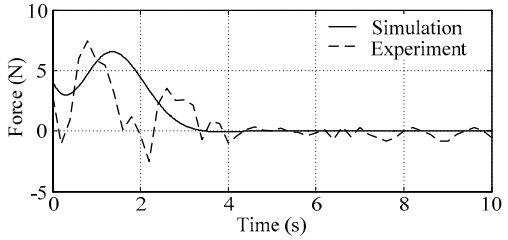

Fig. 14. Trolley driving force.

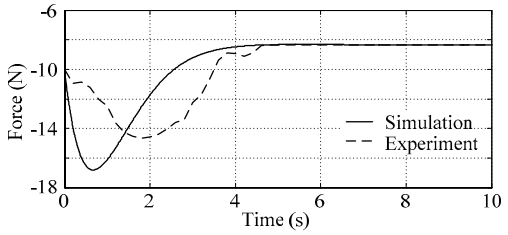

Fig. 15. Payload hoisting force.

the first 1.7 seconds and slows down within the last 2.4 seconds. The cargo is then lifted with increasing speed within the first 0.7 first seconds and with reducing speed within the remaining 3.5 seconds.

The nonlinear control forces are illustrated in Figs. 13-15. The simulation responses achieve steady states after 4, 4.1, and 4.2 seconds for the bridge moving, trolley moving, and the cargo lifting forces, respectively.

At steady states, $u_t^{ss} = u_b^{ss} = 0$ N and $u_l^{ss} = -m_c g = -9.81 \times 0.85 = -8.34$ N.

Obviously, differences in shape still exist between the simulation responses and the experiment responses because the mathematical model and the realistic crane system do not absolutely match. Several nonlinearities that exist in practice, such as the flexibility of cable, the backlash of gears of the reduction box, and nonlinear frictions, are not considered in the mathematical model. Certainly, if the system dynamics is close to a realistic system, then the results will be precise.

Table 2. Response specifications of controllers.

Maximum overshoots and maximum swing angles	PFL	SMC [14]
Bridge motion	0%	5%
Trolley motion	0%	4%
Cargo hoisting motion	0%	0%
Swing angle, θ_{max}	2.9^0	2.9^0
Swing angle, φ_{max}	2.1^0	2.3^0

The nonlinear controllers were previously designed using other control techniques such as SMC, adaptive control, and optimal approach. To investigate the controller quality further, we compare the controller of this study with the SMC controller proposed by Almutairi [14]. Almutairi [14] applied the same type of mathematical model in the controller design as that presented in the current study. The comparison of the response characteristics is shown in Table 2.

The motions of the bridge and trolley controlled by SMC [14] remain at the maximum overshoot. Meanwhile, the maximum overshoots of the PFL-based bridge and trolley motions are completely eliminated. The swing angles of the PFL are also smaller than those of SMC [14].

5. CONCLUSION

The feedback linearization method provides an effective design tool for the control of a class of underactuated mechanical systems such as an overhead crane system. Based on this technique, a quality nonlinear controller was designed. The proposed controller was applied in both simulation analysis and real-time experiment. Both simulation and experiment results show that the proposed controller stabilizes the overhead crane system. All system responses asymptotically reach the desired values within a short period; the bridge and trolley were controlled to move them to the desired position, and the cargo was lifted up to the reference point precisely. Moreover, the cargo swings were kept small during the transfer process and then suppressed at the load destination. In our future work, we will extend this nonlinear control design for the overhead crane by applying the adaptive control technique.

REFERENCES

[1] K.-S. Hong, B. J. Park, and M. H. Lee, "Two-stage control for container cranes," *JSME International Journal*, Series C, vol. 43, no. 2, pp. 273-282, 2000.

[2] Q. H. Ngo and K.-S. Hong, "Skew control of a quay container crane," *Journal of Mechanical Science and Technology*, vol. 23, no. 12, pp. 3332-3339, December 2009.

[3] Q. H. Ngo and K.-S. Hong, "Dynamics of the container crane on a mobile harbor," *Ocean Engineering*, vol. 53, pp. 16-24, 2012.

[4] K. A. F. Moustafa, "Reference trajectory tracking of overhead cranes," *Journal of Dynamics Systems, Measurement, and Control*, vol. 123, no. 1, pp. 139-141, 2001.

[5] D. Chwa, "Nonlinear tracking control of 3D overhead cranes against the initial swing angle and variation of payload weight," *IEEE Trans. on Control Systems Technology*, vol. 17, no. 4, pp. 876-883, 2009.

[6] A. Giua, M. Sanna, and C. Seatzu, "Observer-controller design for three dimensional overhead cranes using time-scaling," *Mathematical and Computer Modeling of Dynamical Systems*, vol. 7, no. 1, pp. 77-107, 2001.

[7] Y. S. Kim, K.-S. Hong, and S. K. Sul, "Anti-sway control of container cranes: inclinometer, observer, and state feedback," *International Journal of Control, Automation, and Systems*, vol. 2, no. 4, pp. 435-449, 2004.

[8] C. S. Kim and K.-S. Hong, "Boundary control of container cranes from the perspective of controlling an axially moving string system," *International Journal of Control, Automation, and Systems*, vol. 7, no. 3, pp. 437-445, 2009.

[9] A. Benhidjeb and G. L. Gissinger, "Fuzzy control of an overhead crane performance comparison with classic control," *Control Engineering Practice*, vol. 3, no. 12, pp. 1687-1696, 1995.

[10] J. Yi, N. Yubazaki, and K. Hirota, "Anti-swing and positioning control of overhead traveling crane," *Information Sciences*, vol. 155, no. 1-2, pp. 19-42, 2003.

[11] C. Y. Chang and K. H. Chiang, "Intelligent fuzzy accelerated method for the nonlinear 3D crane control," *Expert System with Applications*, vol. 35, no. 3, pp. 5750-5752, 2009.

[12] K. T. Hong, C. D. Huh, and K.-S. Hong, "Command shaping control for limiting the transient sway angle of crane systems," *International Journal of Control, Automation, and Systems*, vol. 1, no. 1, pp. 43-53, 2003.

[13] Q. H. Ngo and K.-S. Hong, "Sliding mode anti-sway control of an offshore container crane," *IEEE/ASME Trans. on Mechatronics*, vol. 17, no. 2, pp. 201-209, 2012.

[14] N. Almutairi and M. Zribi, "Sliding mode control of a three dimensional overhead crane," *Journal of Vibration and Control*, vol. 15, no. 11, pp. 1679-1730, 2009.

[15] H. H. Lee, Y. Liang, and D. Segura, "A sliding mode anti-swing trajectory control for overhead cranes with high-speed load hoisting," *Journal of Dynamics Systems, Measurement, and Control*, vol. 128, pp. 842-845, 2006.

[16] G. Bartolini, A. Pisano, and E. Usai, "Second-order sliding mode control of container cranes," *Automatica*, vol. 38, no. 10, pp. 1783-1790, 2002.

[17] Q. H. Ngo and K.-S. Hong, "Adaptive sliding mode control of container cranes," *IET Control Theory and Applications*, vol. 6, no. 5, pp. 662-668, 2012.

[18] Y. Fang, W. E. Dixon, D. M. Dawson, and E. Zergeroglu, "Nonlinear coupling control laws for an under-actuated overhead crane system," *IEEE/ASME Trans. on Mechatronics*, vol. 8, no. 3, pp. 418-423, 2003.

[19] H. C. Cho, J. W. Lee, Y. J. Lee, and K. S. Lee, "Lyapunov theory based robust control of complicated nonlinear mechanical systems with uncertainty," *Journal of Mechanical Science and Technology*, vol. 22, pp. 2142-2150, 2008.
[20] H. H. Lee, "A new approach for the anti-swing control of overhead cranes with high-speed load hoisting," *International Journal of Control*, vol. 76, no. 15, pp. 1493-1499, 2003.
[21] A. Z. Algarni, K. A. F. Moustafa, and S. S. A. K. Javeed Nizami, "Optimal control of overhead cranes," *Control Engineering Practice*, vol. 3, no. 9, pp. 1277-1284, 1995.
[22] G. Corriga and A. Giua, "An implicit gain-scheduling controller for cranes," *IEEE Transactions on Control Systems Technology*, vol. 6, no. 1, pp. 15-20, 1998.
[23] Y. J. Hua and Y. K. Shine, "Adaptive coupling control for overhead crane systems," *Mechatronics*, vol. 17, no. 2-3, pp. 143-152, 2007.
[24] J. H. Yang and S. H. Shen, "Novel approach for adaptive tracking control of a 3D overhead crane system," *Journal of Intelligent Robot System*, vol. 62, no. 1, pp. 59-80, 2010.
[25] Y. Fang, B. Ma, P. Wang, and X. Zhang, "A motion planning-based adaptive control method for an underactuated crane system," *IEEE Transactions on Control System Technology*, vol. 20, no. 1, pp. 241-248, 2012.
[26] N. Sun and Y. Fang, "New energy analytical results for the regulation of underactuated overhead cranes: an end-effector motion based approach," *IEEE Trans. on Industrial Electronics*, vol. 59, no. 12, pp. 4723-4734, 2012.
[27] N. Sun, Y. Fang, X. Zhang, and Y. Yuan, "Transportation task-oriented trajectory planning for underactuated overhead cranes using geometric analysis," *IET Control Theory & Applications*, vol. 6, no. 4, pp. 1410-1423, 2012.
[28] H. Park, D. Chwa, and K.-S. Hong, "A feedback linearization control of Container cranes: varying rope length," *International Journal of Control, Automation, and Systems*, vol. 5, pp. 379-387, 2007.
[29] J. A. Borges, M. A. Botto, and J. S. Costa, "Approximate input-output feedback linearization for the swing cranes system using a state observer," *Proc. of the 10th Mediterranean Conference on Control and Automation*, Lisbon, Portugal, July 2002.
[30] E. Bobasu, D. Selisteanu, D. Popescu, and D. Sendrescu, "On nonlinear adaptive control of a handling crane," *Proc. of the 5th WSEAS International Conference on Simulation, Modeling and Optimization*, Corfu, Greece, August 2005.
[31] H. Chen, B. Gao, and X. Zhang, "Nonlinear controller for a gantry crane based on a partial feedback linearization," *Proc. of International Conference on Control and Automation*, Budapest, Hungary, June 2005.
[32] H. Chen, B. Gao, and X. Zhang, "Dynamical modeling and nonlinear control of a 3D overhead cranes," *Proc. of International Conference on Control and Automation*, Budapest, Hungary, June 2005.
[33] H. C. Cho and K. S. Lee, "Adaptive control and stability analysis of nonlinear crane systems with perturbation," *Journal of Mechanical Science and Technology*, vol. 22, pp. 1091-1098, 2008.
[34] H. C. Cho, J. W. Lee, Y. J. Lee, and K. S. Lee, "Lyapunov theory based robust control of complicated nonlinear mechanical systems with uncertainty," *Journal of Mechanical Science and Technology*, vol. 22, no. 11, pp. 2142-2150, 2008.
[35] H. H. Lee, "Modeling and control of a three-dimensional overhead cranes," *ASME Journal of Dynamic Systems, Measurement, and Control*, vol. 120, no. 4, pp. 471-476, 1998.
[36] T. A. Le, G. H. Kim, M. Y. Kim, and S. G. Lee, "Partial feedback linearization control of overhead cranes with varying cable lengths," *International Journal of Precision Engineering and Manufacturing*, vol. 13, no. 2, pp. 1229-8557, 2012.
[37] T. A. Le, S. C. Moon, W. G. Lee, and S. G. Lee, "Adaptive sliding mode control of the overhead crane with varying cable length," *Journal of Mechanical Science and Technology*, vol. 27, no. 3, pp. 885-893, 2013.

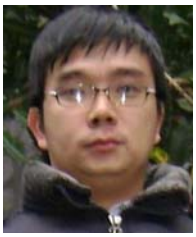

Le Anh Tuan graduated both B.Eng. and M.Eng. in Mechanical Engineering and Marine Machinery from Vietnam Maritime University in 2003 and 2007, respectively. He received his Ph.D. degree in Mechanical Engineering from Kyung Hee University, Korea in 2012. He is a part-time researcher of Duy Tan University, Da Nang, Vietnam. His interested research composes of applied nonlinear control, dynamics and control of industrial machines.

Soon-Geul Lee received his B.E. degree in Mechanical Engineering from Seoul National University, Seoul, Korea; an M.S. degree in Production Engineering from KAIST, Seoul, Korea; and a Ph.D. degree in Mechanical Engineering from the University of Michigan in 1983, 1985 and 1993, respectively. Since 1996, he has been with the Department of Mechanical Engineering of Kyung Hee University, Yongin, Korea, where he is currently a Professor. His research interests include robotics and automation, mechatronics, intelligent control, and biomechanics.

Viet-Hung Dang graduated as an electric-electronics engineer from HoChi-Minh University of Technology in 2003, Vietnam. He got his M.S. from the same university in 2005. He received his Ph.D. degree in Computer Science at Kyung Hee University, Korea in 2012. He is now working for Research and Development Center in Duy Tan University, Vietnam. His research interests are machine learning, artificial intelligence, localization and navigation.

Sangchan Moon received his B.C and M.S degrees in Department of Mechanical Engineering from Kyung Hee University. He is currently pursuing a Ph.D. degree at the Department of Mechanical Engineering, Kyung Hee University. His research interests are in the area of developing a precision positioning system for intelligent vehicle with GPS/INS.

ByungSoo Kim received his B.E. degree in Mechanical Design Engineering from Seoul National University of Science and Technology, Seoul, Korea; his M.S. and Ph.D. degrees in Mechanical Engineering from Kyung Hee University, Yongin, Korea. He is currently as post-doctoral researcher at the Department of Mechanical Engineering, Kyung Hee University. His research interests include humanoid robot, mechatronics, intelligent control, and mobile robot.